A Comparative Analysis of Deterministic Detection and Estimation Techniques for MIMO SFCW Radars

EMILIO SIRIGNANO[iD]**, (Member, IEEE), ALESSANDRO DAVOLI, (Student Member, IEEE), GIORGIO M. VITETTA**[iD]**, (Senior Member, IEEE), AND FEDERICO VIAPPIANI**
Department of Engineering "Enzo Ferrari", University of Modena and Reggio Emilia, 41125 Modena, Italy
Corresponding author: Emilio Sirignano (emilio.sirignano@unimore.it)

ABSTRACT In this paper, the problem of the joint estimation of the range and azimuth of multiple targets in a *multiple-input multiple-output stepped-frequency continuous wave* radar system is investigated. Three deterministic algorithms solving it through an iterative beam cancellation procedure are described; moreover, an iterative technique, based on the *expectation-maximization* algorithm, is developed with the aim of refining their estimates. The accuracy achieved by all the considered algorithms is assessed on the basis of the raw data acquired from a low power wideband radar device. Our results evidence that these algorithms achieve similar accuracies, but at the price of different computational efforts.

INDEX TERMS Beamforming, direction of arrival, multiple-input multiple-output, radar signal processing, stepped-frequency continuous-wave.

I. INTRODUCTION

In recent years, substantial attention has been paid to the development of signal processing techniques for *multiple-input multiple-output* (MIMO) radar systems equipped either with colocated antennas (e.g., see [1]–[7] and references therein) or with distributed antennas (e.g., see [8]–[11] and references therein). Such devices belong to the class of *frequency modulated continuous wave* (FMCW) radars or to that of *stepped frequency continuous wave* (SFCW) radars [12], and operate at 5 GHz, 24 GHz or 77 GHz [13, Ch. 1] . In this paper, we focus on the category of colocated MIMO SFCW radars operating in *time division multiplexing* (TDM) mode and radiating ultra-wideband signals. Our interest in these devices is mainly motivated by their low cost, good sensitivity and ability to resolve closely spaced targets in range; for this reason, their use in various healthcare and through-the-wall applications is currently investigated (e.g., see [14]–[17]). From a signal processing perspective, the detection and estimation algorithms illustrated in the papers cited above are mainly based on the use of: a) *discrete Fourier transform* (DFT) methods for estimating range and *direction of*

The associate editor coordinating the review of this manuscript and approving it for publication was Ahmet M. Elbir.

arrival (DOA) [18], and range and Doppler ; b) standard beamforming methods [14]. All these methods, being deterministic, offer the important advantage of a complexity substantially smaller than that of well known statistical methods like the *multiple signal classification* (MUSIC) technique [21], [22] and the *estimation of signal parameters via rotational invariance technique* (ESPRIT) [23]. However, as far as we know, no paper provides a comparative analysis of various deterministic techniques that can be employed for the detection of multiple targets and the estimation of their range/DOA in colocated MIMO SFCW radars. This paper aims at partly filling this gap, since it investigates a standard beamformer, five *iterative deterministic algorithms*, and analyses their accuracy and complexity. More specifically, in our work, the following iterative algorithms are taken into consideration: a) the so called CLEAN technique [24], [25]; b) the estimation algorithm proposed by Wax and Leshem [26] (dubbed WLA in the following and closely related to the algorithm devised in [27]); c) a *modified* version of the WLA (dubbed MWLA); d) two estimation algorithms based on the combination of the CLEAN and the MWLA with the *expectation-maximization* (EM) technique [28]. These algorithms may play an important role in a number of applications for various reasons; in fact, they process a single
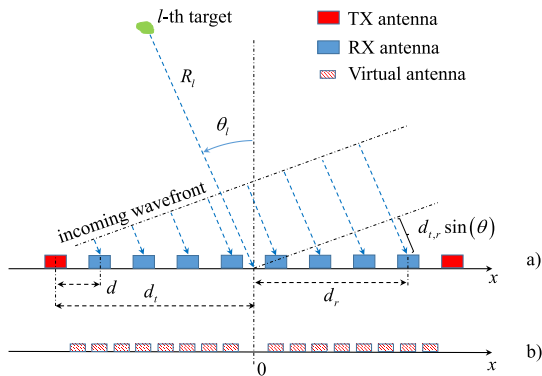
FIGURE 1. Representation of: a) an ULA (characterized by $N_T = 2$ and $N_R = 8$), and the relevant geometric parameters referring to the l-th target, the t-th TX antenna and the r-th RX antenna; b) the associated virtual ULA (consisting of $N_T \cdot N_R = 16$ antennas).

snapshot, in principle do not assume a prior knowledge of the number of targets and, unlike the *maximum likelihood* (ML) approach, involve *one-dimensional* (1D) or *two-dimensional* (2D) maximizations only. Moreover, our numerical results, based on the experimental data acquired from a low-power radar device, show that they are able to achieve a good accuracy at a reasonable computational cost. It is also important to point out that: 1) as far as we know, the application of the standard beamformer and of the CLEAN technique to SFCW radars has not been investigated previously; 2) the WLA has been originally proposed for range and DOA estimation in a narrowband system and its adaptation to a wideband radar system is analyzed for the first time in this paper; 3) the MWLA and the estimation algorithms based on combining the CLEAN algorithm (or the MWLA) with the EM technique are new. The remaining part of this paper is organized as follows. The models of the considered radar array and of the measurements acquired through it in a MIMO SFCW radar are illustrated in Section II. The above mentioned estimation methods are described in Section III. Various numerical results about the accuracy achieved by such methods and their computational requirements are shown in Section IV. Finally, some conclusions are offered in Section V.

II. ANTENNA ARRAY AND SIGNAL MODELS
In this Section we focus on a MIMO SFCW radar system and describe the models adopted for its antenna array and the received signal.

A. ARRAY MODEL
In the following we consider a colocated SFCW radar system equipped with a *uniform linear array* (ULA) and operating in a *two-dimensional* (2D) propagation scenario for simplicity; an example of ULA, consisting of two *transmit* (TX) antennas and eight *receive* (RX) antennas, is provided in Fig. 1-a) (where the inter-antenna spacing is denoted d). We also assume that the employed array consists of N_T TX antennas and N_R RX antennas, so that $(N_T + N_R)$ physical elements are available. Therefore, a *virtual* array, consisting of $N_T \cdot N_R$

virtual elements, can be defined and exploited in processing the available measurements acquired through the physical receive antennas [29]. In the considered scenario, the abscissa $x_{t,r}$ of the *virtual element* associated with the t-th TX antenna and the r-th RX antenna is computed as

$$x_{t,r} = \frac{x_t + x_r}{2}, \qquad (1)$$

with $t = 1, 2, \ldots, N_T$ and $r = 1, 2, \ldots, N_R$; here, x_t (x_r) denotes the abscissa of the considered TX (RX) antenna. For instance, given the physical ULA illustrated in Fig. 1-a), the virtual ULA shown in Fig. 1-b) can be easily generated.

B. RECEIVED SIGNAL MODEL
The MIMO radar system considered in this paper provides, for any couple of TX and RX antennas, a set of N_f measurements in the frequency domain; each measurement represents an estimate of the frequency response of the communication channel between such antennas at a specific frequency. In practice, these measurements are acquired by sounding the communication channel at N_f equally spaced frequencies; in our work, the n-th frequency (with $n = 0, 1, \ldots, N_f - 1$) is evaluated as

$$f_n = f_0 + n \cdot \Delta f, \qquad (2)$$

where f_0 and Δf denote the smallest carrier frequency of the radiated signal and the step size, respectively. If the t-th (r-th) antenna is selected for transmission (reception) and the presence of L targets (i.e., detectable echoes) is assumed, the radar generates the estimate

$$\hat{H}_{t,r}[n] = \sum_{l=0}^{L-1} h_l \exp\left(-j2\pi f_n \tau_{t,r}[l]\right) + n_{t,r}[n], \qquad (3)$$

of the frequency response $H_{t,r}(f)$ characterizing the communication channel between the considered antennas at the frequency f_n; here, h_l and $\tau_{t,r}[l]$ denote the complex amplitude (accounting for both attenuation and phase shift) and the overall delay, respectively, characterizing the l-th target, and $n_{t,r}[n]$ represents the *additive white Gaussian noise* (AWGN) affecting the considered estimate. In the following, we assume that: a) the inequality $|h_l| \geq |h_{l+1}|$ holds for $l = 0, 1, \ldots, L-2$, so that the received echoes are ordered according to decreasing strenghts; b) all the targets are in far field; c) the range R_l and the azimuth θ_l of the l-th target (with $l = 0, 1, \ldots, N-1$) are measured with respect to the centre of the array, as illustrated in Fig. 1-a). The last two assumptions allow us to express the delay $\tau_{t,r}[l]$ appearing in the *right-hand side* (RHS) of eq. (3) as

$$\tau_{t,r}[l] = \tau_l + \Delta\tau_{t,r}[l], \qquad (4)$$

where $\tau_l = 2R_l/c$ represents the round-trip delay associated with the distance R_l (see Fig. 1-a)) and

$$\Delta\tau_{t,r}[l] = \frac{d_r - d_t}{c} \sin(\theta_l)$$
$$= \frac{x_r + x_t}{c} \sin(\theta_l) = \frac{2x_{t,r}}{c} \sin(\theta_l), \qquad (5)$$

represents the contribution of the spacing between the centre of the virtual array (identified by the symbol '0' in Fig. 1-b) and coincident with the centre of the physical array shown in Fig. 1-a)), and the virtual antenna associated with the t-th TX and the r-th RX physical elements. In the last formula, c denotes the speed of light, and d_t (d_r) represents the distance of the t-th TX (r-th RX) antenna from the centre of the array (note that the difference ($d_r - d_t$) is denoted $d_{t,r}$ in Fig. 1-a)).

Substituting eq. (4) in the RHS of eq. (3) yields

$$\tilde{H}_{t,r}[n] = \sum_{l=0}^{L-1} h_l a_{t,r}(\theta_l, f_n) b(\tau_l, f_n) + n_{t,r}[n], \quad (6)$$

where $a_{t,r}(\theta_l, f_n) \triangleq \exp(-j2\pi f_n \Delta\tau_{t,r}[l])$ and $b(\tau_l, f_n) \triangleq \exp(-j2\pi f_n \tau_l)$. Then, if the measurements are acquired from multiple (say, $N_R[t]$) RX antennas when the sounding signal is radiated by the t-th TX antenna, the $N_R[t]$-dimensional measurement vector

$$\tilde{\mathbf{H}}_t[n] \triangleq \left[\tilde{H}_{t,r_1}[n], \tilde{H}_{t,r_2}[n], \ldots, \tilde{H}_{t,r_{N_R[t]}}[n] \right]^T \quad (7)$$

$$= \sum_{l=0}^{L-1} h_l \mathbf{a}_t(\theta_l, f_n) b(\tau_l, f_n) + \mathbf{n}_t[n], \quad (8)$$

becomes available at the frequency f_n; here, $\mathbf{n}_t[n] \triangleq [n_{t,r_1}[n], n_{t,r_2}[n], \ldots, n_{t,r_{N_R[t]}}[n]]^T$ is a noise vector, whereas $\mathbf{a}_t(\theta_l, f_n) \triangleq [a_{t,r_1}(\theta_l, f_n), a_{t,r_2}(\theta_l, f_n), \ldots, a_{t,r_{N_R[t]}}(\theta_l, f_n)]^T$ denotes the *steering vector* associated with the azimuth θ_l and the frequency f_n.

III. RANGE AND DOA ESTIMATION ALGORITHMS
In this Section, we first provide various mathematical details about the range and azimuth estimation algorithms developed in our work (see Subsections III-A-D); then, we illustrate their computational complexity (see Subsection III-E). In the following, we always assume, for simplicity, that a single transmit antenna (in particular, the t-th TX antenna) and multiple (namely, $N_R[t]$) receive antennas are exploited for range and DOA estimation.

A. STANDARD BEAMFORMER
The standard beamforming algorithm employed in our work is based on the *cost function* (e.g., see [25] and [30])

$$J_t(\tilde{\theta}, \tilde{\tau}) \triangleq \left| S_t(\tilde{\theta}, \tilde{\tau}) \right|^2, \quad (9)$$

where

$$S_t(\tilde{\theta}, \tilde{\tau}) \triangleq \sum_{n=0}^{N_f-1} \sum_{k=1}^{N_R[t]} \tilde{H}_{t,r_k}[n] a_{t,r_k}^*(\tilde{\theta}, f_n) b^*(\tilde{\tau}, f_n). \quad (10)$$

It is well known that the cost function $J_t(\tilde{\theta}, \tilde{\tau})$ (9) describes the power density distribution of the received signal versus the azimuth $\tilde{\theta}$ and the delay $\tilde{\tau}$. For this reason, estimates of the target parameters $\{(\theta_l, \tau_l)\}$ (and also, approximately, of the gains $\{h_l\}$) can be computed by identifying the positions of

its local maxima; note also that, if a local maximum is found at $(\tilde{\theta}, \tilde{\tau}) = (\hat{\theta}, \hat{\tau})$, the estimate

$$\hat{h} = \frac{S_t(\hat{\theta}, \hat{\tau})}{N_f \cdot N_R[t]} \quad (11)$$

of the complex gain h associated with the corresponding target can be easily evaluated. The most computationally demanding task in the implementation of this algorithm is represented by the identification of the peaks of the function $J_t(\tilde{\theta}, \tilde{\tau})$ (9); in practice, this requires accomplishing a search over a sufficiently fine rectangular grid in a 2D space. If the elements of the antenna array are uniformly spaced and a uniform grid is employed, the evaluation of the function $S_t(\tilde{\theta}, \tilde{\tau})$ (10) over such a grid can be efficiently accomplished by means of a 2D DFT of proper order. However, independently of the selected order, the resolution of this method in both range and azimuth is limited by the fact that the contributions of weak echoes might not be visible in the presence of strong echoes due to spatially close targets; in fact, the local maxima originating from the former echoes might be hidden by the sidelobes associated with the latter ones. These considerations motivate the use of the estimation algorithms described in the following two subsections.

B. THE CLEAN ALGORITHM
In this subsection, the so called CLEAN algorithm, originally proposed by Högbom [24] for radio astronomy applications, is adapted to the measurement model (3) and the cost function $J_t(\tilde{\theta}, \tilde{\tau})$ (9). The resulting algorithm exploits the same cost function as standard beamforming but, unlike it, employs an iterative beam-removing process. This means that, within each iteration of this algorithm, the parameters of a new target are estimated and the contribution of this target (together with those due to the targets identified in the previous iterations) are subtracted from the function $S_t(\tilde{\theta}, \tilde{\tau})$ (10). Then, this resulting residual function is passed to the next iteration, where it is processed to identify a new target. The processing tasks executed by the CLEAN algorithm can be divided in six steps; a detailed description of each of them is provided below.

1) *Initialization* - Set the iteration index l to 0 and define (see eq. (7))

$$\tilde{\mathbf{H}}_t^{(0)}[n] \triangleq \left[\tilde{H}_{t,r_1}^{(0)}[n], \tilde{H}_{t,r_2}^{(0)}[n], \ldots, \tilde{H}_{t,r_{N_R[t]}}^{(0)}[n] \right]^T$$

$$= \tilde{\mathbf{H}}_t[n]. \quad (12)$$

for $n = 0, 1, \ldots, N_f - 1$.

2) *Computation of the cost function over a rectangular grid* - Compute the cost function (see eq. (9))

$$J_t^{(l)}(\tilde{\theta}, \tilde{\tau}) \triangleq \left| \tilde{S}_t^{(l)}(\tilde{\theta}, \tilde{\tau}) \right|^2, \quad (13)$$

for $\tilde{\theta} = \theta_k \triangleq \theta_0 + k\Delta\theta$ (with $k = 0, 1, \ldots, N_\theta - 1$) and $\tilde{\tau} = \tau_p \triangleq \tau_0 + p\Delta\tau$ (with $p = 0, 1, \ldots, N_\tau - 1$); here,

the function $\tilde{S}_t^{(l)}(\tilde{\theta}, \tilde{\tau})$ is defined as (see eq. (10))

$$\tilde{S}_t^{(l)}\left(\tilde{\theta}, \tilde{\tau}\right) \triangleq \sum_{n=0}^{N_f-1} \sum_{k=1}^{N_R[t]} \tilde{H}_{t,r_k}^{(l)}[n]\, a_{t,r_k}^*(\tilde{\theta}, f_n) b^*(\tilde{\tau}, f_n), \quad (14)$$

and θ_0 (τ_0), $\Delta\theta$ ($\Delta\tau$) and N_θ (N_τ) represent the lower limit of the search interval considered for azimuth (delay), the step size for the variable $\tilde{\theta}$ ($\tilde{\tau}$) and the overall number of values selected for $\tilde{\theta}$ ($\tilde{\tau}$). In our work, $\tau_0 = 2R_m/c$, $\tau_{N_\tau-1} = 2R_M/c$ and $\Delta\tau = 2\Delta R/c$ have been selected, where R_m, R_M and ΔR represent the minimum value, the maximum value and the step size, respectively, for the trial value of target range.

3) *Estimation of the parameters of a new target* - Perform the search for the global maximum over the set $\{J_t^{(l)}(\tilde{\theta}_k, \tilde{\tau}_p)\}$ (consisting of $N_\theta \cdot N_\tau$ values); the coordinates of the point associated with the global maximum are denoted $(\hat{\theta}_l, \hat{\tau}_l)$. Then, compute the estimate (see eq. (11))

$$\hat{h}_l = \frac{S_t^{(l)}(\hat{\theta}_l, \hat{\tau}_l)}{N_f \cdot N_R[t]} \quad (15)$$

of h_l and store the estimates $(\hat{h}_l, \hat{\theta}_l, \hat{\tau}_l)$.

4) *Threshold test for identifying false targets* - If

$$|\hat{h}_l| < T, \quad (16)$$

where T denotes a proper (positive) threshold, go to step 6); otherwise, proceed with the next step.

5) *Cancellation of the last identified target* - Cancel the contribution of the last target in the measured frequency response by computing the *residual frequency response*

$$\tilde{H}_t^{(l+1)}[n] \triangleq \tilde{H}_t^{(l)}[n] - \hat{h}_l \mathbf{a}_t(\hat{\theta}_l, f_n) b\left(\hat{\tau}_l, f_n\right), \quad (17)$$

for $n = 0, 1, \ldots, N_f - 1$. Then, increase the iteration index l by one and go to step 2);

6) *End* - The final output provided by the algorithm is expressed by the set of values $\{(\hat{\theta}_l, \hat{\tau}_l, \hat{h}_l); l = 0, 1, \ldots, \bar{L} - 1\}$, where $\bar{L}$, the estimate of L, is given by the last value taken on by the index l.

It is important to point out that, before executing the CLEAN algorithm, a proper value for the threshold T appearing in eq. (16) must be selected. In fact, on the one hand, relevant echoes might be missed if T is too large; on the other hand, false targets might be identified if T is too small. This problem can be circumvented by estimating L before running the CLEAN algorithm (so that step 4) is no more accomplished). In principle, this result can be achieved by exploiting the *minimum description length* (MDL) method [31] or the *Akaike Information Criterion* (AIC) [32]; in practice, however, this entails a significant computational cost. Finally, it is worth mentioning that the cancellation procedure expressed by eq. (17) may suffer from error accumulation; this is due to the fact that the effects of estimation errors accumulate over successive iterations. This may result in poor accuracy; in particular, in the presence of multiple and/or closely spaced targets this could even result in the identification of false targets.

C. THE WAX AND LESHEM ESTIMATION METHOD

In this subsection, we first describe a specific instance of the estimation algorithm proposed by Wax and Leshem [26] (this algorithm is dubbed WLA in the following); then, we show how this method can be modified to solve the numerical problems experienced in its use.

The WLA is an iterative method devised to solve the problem of jointly estimating the DOA's and the time delays of multiple reflections occurring in a 2D multi-target scenario, in which a known *narrowband* signal is transmitted; its main feature is represented by the fact that it requires solving *one-dimensional* (1D) optimizations only. Despite the differences between the scenario described in [26, Sec. II] and the one considered in this paper (in which a *wideband* signal is radiated), this algorithm can be properly modified to solve our estimation problem since: 1) it operates in the frequency domain (in fact, it processes the output of a DFT fed by the time domain samples of the received signal); b) the structure of the received signal vector in the frequency domain is similar to the one adopted for $\tilde{H}_t[n]$ (6) (the structures become equivalent if we set $s(\omega_k) = 1$ in eq. (9) of [26, Sec. III]). A detailed derivation of the formulas employed by the WLA can be found in [26, Sec. IV]; in the following, we limit to summarise the steps it consists of and to illustrate the employed formulas. Similarly as the CLEAN algorithm, the WLA, in each of its iterations, estimates the parameters of a new target; however, unlike the CLEAN algorithm, the WLA updates the estimates of the parameters related with the previously identified targets. Let us assume now that, at beginning of the l-th iteration of the WLA (with $l = 1, 2, \ldots$), the estimates $\{(\hat{h}_k^{(l-1)}, \hat{\theta}_k^{(l-1)}, \hat{\tau}_k^{(l-1)}), k = 0, 1, \ldots, l-1\}$ of the l triplets $\{(h_k, \theta_k, \tau_k), k = 0, 1, \ldots, l-1\}$ are available. Then, the processing accomplished within this iteration evolves through the four steps described below.

1. *Coarse estimation of a new DOA* - In this step, a *coarse* estimate $\check{\theta}_l^{(l)}$ of the azimuth θ_l referring to the new (i.e., to the l-th) target is computed on the basis of the *alternating projection* method illustrated in [27]. This requires:
a) computing the $N_R[t] \times N_R[t]$ *covariance matrix*

$$\mathbf{R}_{xx}^{(l)} \triangleq \frac{1}{N_f} \sum_{n=0}^{N_f-1} \tilde{H}_t^{(l)}[n] \left(\tilde{H}_t^{(l)}[n]\right)^H \quad (18)$$

of the *residual* channel response

$$\tilde{H}_t^{(l)}[n] \triangleq \tilde{H}_t[n] - \sum_{k=0}^{l-1} \hat{h}_k^{(l-1)} b\left(\hat{\tau}_k^{(l-1)}, f_n\right) \mathbf{a}_t(\hat{\theta}_k^{(l-1)}, f_n); \quad (19)$$

b) defining the *orthogonal projection matrix*

$$\mathbf{P}\left(\tilde{\boldsymbol{\theta}}^{(l)}\right) \triangleq \mathbf{A}_t\left(\tilde{\boldsymbol{\theta}}^{(l)}\right) \mathbf{D}_t\left(\tilde{\boldsymbol{\theta}}^{(l)}\right)^{-1} \mathbf{A}_t\left(\tilde{\boldsymbol{\theta}}^{(l)}\right)^H, \quad (20)$$

where

$$\mathbf{A}_t\left(\boldsymbol{\theta}^{(l)}\right) \triangleq [\mathbf{a}_t\left(\theta_0, f_r\right), \mathbf{a}_t\left(\theta_1, f_r\right), \ldots, \mathbf{a}_t(\theta_l, f_r)], \quad (21)$$

is a $N_R[t] \times (l+1)$ matrix, $\mathbf{D}_t(\boldsymbol{\theta}^{(l)}) \triangleq \mathbf{A}_t^H(\tilde{\boldsymbol{\theta}}^{(l)})\mathbf{A}_t(\tilde{\boldsymbol{\theta}}^{(l)})$, $\boldsymbol{\theta}^{(l)} \triangleq [\theta_0, \theta_1, \ldots, \theta_l]$, $\tilde{\boldsymbol{\theta}}^{(l)} \triangleq [\hat{\theta}_0^{(l-1)}, \hat{\theta}_1^{(l-1)}, \ldots, \hat{\theta}_{l-1}^{(l-1)}, \tilde{\theta}]$ and f_r

is a proper *reference frequency* (in our work, f_r is always equal to the central frequency f_c of the wideband radiated signal). In fact, given the matrices $\mathbf{R}_{xx}^{(l)}$ (18) and $\mathbf{P}(\tilde{\boldsymbol{\theta}}^{(l)})$ (20), the estimate $\check{\theta}_l^{(l)}$ is computed as

$$\check{\theta}_l^{(l)} = \arg\max_{\tilde{\theta} \in S_{\tilde{\theta}}} \operatorname{tr}\left(\mathbf{P}\left(\tilde{\boldsymbol{\theta}}^{(l)}\right) \mathbf{R}_{xx}^{(l)}\right), \qquad (22)$$

where $S_{\tilde{\theta}} = [\theta_0, \theta_{N_\theta - 1}]$ is the search interval considered for the azimuth of the new target, θ_0 and $\theta_{N_\theta - 1}$ represent its lower and upper limits, respectively, and $\operatorname{tr}(\mathbf{X})$ denotes the trace of the square matrix $\mathbf{X}$.

2. *Estimation of target delays* - In this step, an estimate $\hat{\tau}_k^{(l)}$ of the delay τ_k (with $k = 0, 1, \ldots, l$) is evaluated by solving $(l + 1)$ 1D optimization problems. This requires computing first the $(l + 1)$-dimensional column vector

$$\hat{\mathbf{u}}_{t,k}^{(l)}[n] \triangleq \mathbf{D}_t\left(\check{\boldsymbol{\theta}}_k^{(l)}\right)^{-1} \mathbf{A}_t\left(\check{\boldsymbol{\theta}}_k^{(l)}\right)^H \tilde{\mathbf{H}}_t^{(l)}[n], \qquad (23)$$

with $n = 0, 1, \ldots, N_f - 1$; here, $\check{\boldsymbol{\theta}}_k^{(l)} \triangleq [\hat{\theta}_0^{(l-1)}, \hat{\theta}_1^{(l-1)}, \ldots, \hat{\theta}_{l-1}^{(l-1)}, \check{\theta}_l^{(l)}]$. Then, the $N_f \times (l+1)$ matrix $\hat{\mathbf{v}}_{t,k}^{(l)}$ is generated by stacking the N_f row vectors $\{(\hat{\mathbf{u}}_{t,k}^{(l)}[n])^T, n = 0, 1, \ldots, N_f - 1\}$ according to their natural order. Finally, $\hat{\tau}_k^{(l)}$ is computed as

$$\hat{\tau}_k^{(l)} = \arg\max_{\tilde{\tau} \in S_{\tilde{\tau}}} \left\| \mathbf{b}^H\left(\tilde{\tau}, f_n\right) \hat{\mathbf{v}}_{t,k}^{(l)} \right\|^2 \qquad (24)$$

for $k = 0, 1, \ldots, l$, where $S_{\tilde{\tau}} \triangleq [2R_m/c, 2R_M/c]$, and $\|\mathbf{X}\|$ denotes the Euclidean norm of the complex vector $\mathbf{X}$.

3. *Fine estimation of target DOA's* - In this step, a fine estimate $\hat{\theta}_k^{(l)}$ of θ_k (with $k = 0, 1, \ldots, l$) is evaluated by solving $(l + 1)$ 1D optimization problems. More specifically, $\hat{\theta}_k^{(l)}$ is computed as

$$\hat{\theta}_k^{(l)} = \arg\max_{\tilde{\theta} \in S_{\tilde{\theta}}} \|\mathbf{A}_t^H(\check{\boldsymbol{\theta}}_k^{(l)})\hat{\mathbf{B}}_{t,k}^{(l)}\|^2, \qquad (25)$$

where $\check{\boldsymbol{\theta}}_k^{(l)} \triangleq [\hat{\theta}_0^{(l)}, \ldots, \hat{\theta}_{k-1}^{(l)}, \tilde{\theta}, \hat{\theta}_{k+1}^{(l-1)}, \ldots, \hat{\theta}_l^{(l-1)}]$, $\hat{\mathbf{B}}_{t,k}^{(l)}$ denotes the k-th column of the $N_R[t] \times (l + 1)$ matrix

$$\hat{\mathbf{B}}_t^{(l)} = \left[\sum_{n=0}^{N_f - 1} \tilde{\mathbf{H}}_t[n]\mathbf{r}^H\left(n, \hat{\tau}^{(l)}\right)\right]\left(\hat{\mathbf{C}}^{(l)}\right)^{-1}, \qquad (26)$$

$$\mathbf{r}\left(n, \hat{\tau}^{(l)}\right) \triangleq \left[b\left(\hat{\tau}_0^{(l)}, f_n\right), b\left(\hat{\tau}_1^{(l)}, f_n\right), \cdots, b\left(\hat{\tau}_l^{(l)}, f_n\right)\right]^T \qquad (27)$$

is an $(l+1)$-dimensional column vector, $\hat{\tau}^{(l)} \triangleq [\hat{\tau}_0^{(l)}, \hat{\tau}_1^{(l)}, \cdots, \hat{\tau}_l^{(l)}]$ is an $(l + 1)$-dimensional row vector and

$$\hat{\mathbf{C}}^{(l)} \triangleq \sum_{n=0}^{N_f - 1} \mathbf{r}\left(n, \hat{\tau}^{(l)}\right) \mathbf{r}^H\left(n, \hat{\tau}^{(l)}\right) \qquad (28)$$

is a $(l + 1) \times (l + 1)$ matrix.

4. *Estimation of target gains* - In this step, the estimate

$$\hat{h}_k^{(l)} = \left\|\mathbf{A}_t\left(\hat{\theta}_k^{(l)}\right)\right\|^{-2} \mathbf{A}_t^H\left(\hat{\theta}_k^{(l)}\right) \hat{\mathbf{B}}_{t,k}^{(l)} \qquad (29)$$

of the complex gain h_k is computed for $k = 0, 1, \ldots, l$; here, $\hat{\boldsymbol{\theta}}_k^{(l)} \triangleq [\hat{\theta}_0^{(l)}, \hat{\theta}_1^{(l)}, \ldots, \hat{\theta}_l^{(l)}]$ and $\|\mathbf{A}_t(\hat{\boldsymbol{\theta}}_k^{(l)})\|^2 = N_f \cdot N_R[t]$ ($\|\mathbf{A}_t(\hat{\boldsymbol{\theta}}_k^{(l)})\|^2 = N_R[t]$ if a single frequency is considered). This concludes the l-th iteration.

The WLA is initialized as follows. A coarse estimate $\check{\theta}_0^{(0)}$ of the first DOA (i.e., of the DOA referring to the dominant target) is computed by means of eq. (22), where the covariance matrix $\mathbf{R}_{xx}^{(0)}$ refers to the vector $\tilde{\mathbf{H}}_t^{(0)}[n] = \tilde{\mathbf{H}}_t[n]$ for any n (see eq. (7)) and $\mathbf{A}_t(\tilde{\theta}_0) \triangleq \mathbf{a}_t(\theta_0, f_r)$ is employed in the evaluation of the projection matrix $\mathbf{P}(\tilde{\boldsymbol{\theta}}^{(l)})$ (20). Then, the initial estimates $\hat{h}_0^{(0)}$ and $\hat{\tau}_0^{(0)}$ of the gain h_0 and the delay τ_0, respectively, are computed on the basis of the procedure illustrated in the second and fourth steps, respectively.

This algorithm deserves various comments. First of all, it is worth mentioning that steps 2. and 3. can be repeated multiple times within the l-th iteration of the WLA (before executing step 4.) in order to progressively refine the estimates of both the delays and the DOA's; however, this results in an increase of the overall computational cost. Second, a method for limiting the number of iterations accomplished by the WLA is required. In this case, similarly as the CLEAN algorithm, the MDL or the AIC techniques can be employed to estimate L *before* executing the WLA. However, a simpler alternative to this approach, based on the evaluation of the energy

$$E_{\tilde{H}}^{(l)} = \sum_{n=0}^{N_f - 1} \left\|\tilde{\mathbf{H}}_t^{(l)}[n]\right\|^2 \qquad (30)$$

of the residual channel response $\tilde{\mathbf{H}}_t^{(l)}[n]$ (19) at the beginning of the l-th iteration (with $l > 1$), can be employed for estimating L within the WLA. In fact, the new approach consists in stopping the WLA if

$$E_{\tilde{H}}^{(l-1)} - E_{\tilde{H}}^{(l)} < \varepsilon_{\tilde{H}}, \qquad (31)$$

where $\varepsilon_{\tilde{H}}$ is a proper threshold; this means that the new cancellation (see eq. (19)), based on the parameters of the target identified in the last (i.e., in the $(l-1)$-th iteration), has not resulted in a significant reduction of the residual energy.

Even if the WLA illustrated above is based on a rigorous derivation, our simulations have evidenced that, in our application, it cannot be employed as it is, since it suffers from severe ill-conditioning in the presence of multiple and highly correlated impinging signals. In fact, when this occurs, some columns of the matrix $\mathbf{A}_t(\check{\boldsymbol{\theta}}^{(l)})$ (21) are similar and this makes the computation of the projection matrix $\mathbf{P}(\tilde{\boldsymbol{\theta}}^{(l)})$, of the vectors $\{\hat{\mathbf{u}}_{t,k}^{(l)}\}$ and, consequently, of the estimates $\{\hat{\boldsymbol{\tau}}^{(l)}\}$ (see eqs. (20), (23) and (24), respectively) inaccurate; this results in a poor accuracy in DOA estimation. In our work, to circumvent this problem, the WLA has been modified in way that, when estimating the parameters of a new target, the presence of all the previously identified targets is accounted for in the evaluation of the residual $\tilde{\mathbf{H}}_t^{(l)}[n]$ only (see eq. (19)). This means that, in the l-th iteration, the availability of the estimates $(\hat{h}_l, \hat{\theta}_l, \hat{\tau}_l)$ computed for l-th target is not exploited to refine the estimates associated with the other

detected targets. For this reason, the following changes are introduced in the WLA:

a) In step 1., the residual $\tilde{\mathbf{H}}_t^{(l)}[n]$ is computed on the basis of the recursive formula

$$\tilde{\mathbf{H}}_t^{(l)}[n] \triangleq \tilde{\mathbf{H}}_t^{(l-1)}[n] - \hat{h}_{l-1} b\left(\hat{\tau}_{l-1}, f_n\right) \mathbf{a}_t(\hat{\theta}_{l-1}, f_r), \quad (32)$$

(which is employed in place of eq. (19)) and the matrix $\mathbf{A}_t(\check{\boldsymbol{\theta}}^{(l)})$ (21) is replaced by the vector $\mathbf{a}_t(\tilde{\theta}, f_c)$ (with $\tilde{\theta} \in S_{\tilde{\theta}}$) when computing the projection matrix $\mathbf{P}(\tilde{\theta})$ (see eq. (20)); consequently, the optimization problem (22) can be reformulated as (see [27, Sect. IV] for a proof)

$$\check{\theta}_l = \arg \max_{\tilde{\theta} \in S_\theta} \mathbf{a}_{t,n}^H(\tilde{\theta}, f_r) \mathbf{R}_{xx}^{(l)} \mathbf{a}_{t,n}(\tilde{\theta}, f_r), \quad (33)$$

where $\mathbf{a}_{t,n}(\tilde{\theta}, f_r) \triangleq ||\mathbf{a}_t(\tilde{\theta}, f_r)||^{-1} \mathbf{a}_t(\tilde{\theta}, f_r)$ and $\check{\theta}_l$ corresponds to $\check{\theta}_l^{(l)}$.

b) In step 2., the matrix $\mathbf{A}_t(\check{\boldsymbol{\theta}}_k^{(l)})$ is replaced by the vector $\mathbf{a}_t(\check{\theta}_l, f_c)$ in computing the vector $\hat{\mathbf{u}}_{t,l}^{(l)}$ on the basis of eq. (23).

c) In step 3., the vector $\mathbf{r}(n, \hat{\tau}^{(l)})$ (27) is replaced by the scalar $b(\hat{\tau}_l^{(l)}, f_n)$ in the evaluation of the matrix $\hat{\mathbf{C}}^{(l)}$(28) (that turns into a scalar too) and of the matrix $\hat{\mathbf{B}}_{t,k}^{(l)}$ (26).

The estimation algorithm resulting from all these modifications is called *modified* WLA (MWLA) in the following. It is worth mentioning that:

1. The frequency domain cancellation formula (19) employed in the MWLA is similar to that adopted in the CLEAN algorithm (see eq. (17)). For this reason, the accuracy of the MWLA is also affected by the phenomenon of error accumulation described at the end of subsection III-B.

2. In the l-th iteration of the MWLA, the parameters estimated for the l-th target can be progressively refined by repeating steps 2. and 3. multiple times. However, in this case, the modified versions of eqs. (24) and (25) are employed for $k = l$ only.

3. The MWLA is faster than the CLEAN algorithm; this is mainly due to the fact that the former algorithm, unlike the latter one, requires solving only 1D optimizations and does not always exploit the information available at the N_f frequencies (for instance, the projection matrix $\mathbf{P}(\tilde{\boldsymbol{\theta}}^{(l)})$ (20) is computed at the reference frequency only). Moreover, our computer simulations have evidenced that the MWLA is numerically stable and much faster than the WLA and that, despite the substantial simplifications adopted in its derivation, achieves a good accuracy.

D. AN EM-BASED ALGORITHM FOR REFINING THE ESTIMATES OF TARGET PARAMETERS

As illustrated in the previous two subsections, the estimates $\{(\hat{\theta}_k, \hat{\tau}_k, \hat{h}_k); k = 0, 1, \ldots, l\}$, referring to l distinct targets, are available at the end of the l-th iteration of both the CLEAN algorithm and the MWLA. However, unlike the WLA, no attempt is made in these two algoritms to refine the estimates $\{(\hat{\theta}_k, \hat{\tau}_k, \hat{h}_k); k = 0, 1, \ldots, l-1\}$ computed in the previous iterations, once the new estimate $(\hat{\theta}_l, \hat{\tau}_l, \hat{h}_l)$ becomes available at the end of the l-th iteration. Moreover,

as already mentioned at the end of the previous subsection, the MWLA does not fully exploit the information available at all the transmitted frequencies, since part of its processing involves the measurements acquired at a reference frequency only; this may substantially affect its accuracy.

These considerations have motivated the work illustrated in this subsection and concerning the development of a computationally efficient technique that, based on the whole set of available measurements, can refine the estimates made available by the CLEAN algorithm or by the MWLA at the end of a) each iteration or b) their final iteration. The technique we have developed for this task is based on the EM algorithm [28] and has been inspired by the fact that, for a given l, the n-th measurement $\tilde{H}_{t,r}[n]$ (6) acquired on the r-th RX antenna can seen as the superposition of $(l + 1)$ distinct *deterministic* samples $\{h_k a_{t,r}(\theta_k, f_n) b(\tau_k, f_n); k = 0, 1, \ldots, l\}$ (characterized by the parameters $\{(h_k, \theta_k, \tau_k), k = 0, 1, \ldots, l\}$) with a noise sample (including the contribution of both the AWGN and the $(L - 1 - l)$ ignored targets). For this reason, the frequency domain measurement model (6) is structurally similar to the time domain model expressed by eq. (50) in ref. [33, Sect. IV] and referring to the case in which a deterministic waveform is received in the presence of channel noise and multipath. This similarity allows us to develop an EM-based iterative algorithm (called EM–*based estimator*, EMBE) potentially able to refine the estimates of the parameters $\{(\theta_k, \tau_k, h_k), k = 0, 1, \ldots, l\}$ starting from their initial values $\{(\hat{\theta}_k, \hat{\tau}_k, \hat{h}_k); k = 0, 1, \ldots, l\}$. Each of the EMBE iterations consists of an *estimation* (E) step, followed by a *maximization* (M) step; such steps are described below for the p-th iteration (with $p = 1, 2, \ldots, N_{EM}$, where N_{EM} denotes the overall number of iterations).

E step - This step aims at computing the $N_R[t] \times N_f$ matrix

$$\mathbf{X}_t^{(p)}[k] = \hat{\mathbf{H}}_t\left(\tilde{h}_k^{(p-1)}, \tilde{\theta}_k^{(p-1)}, \tilde{\tau}_k^{(p-1)}\right)$$
$$+ \beta_k^{(l)} \left[\tilde{\mathbf{H}}_t - \sum_{q=0}^{L-1} \hat{\mathbf{H}}_t\left(\tilde{h}_q^{(p-1)}, \tilde{\theta}_q^{(p-1)}, \tilde{\tau}_q^{(p-1)}\right)\right]$$
$$(34)$$

for $k = 0, 1, \ldots, l$; here, $(\tilde{\theta}_q^{(p-1)}, \tilde{\tau}_q^{(p-1)}, \tilde{h}_q^{(p-1)})$ denotes the estimate of (θ_q, τ_q, h_q) computed in the previous (i.e., in the $(p-1)$-th) iteration of the EMBE for any q, $\tilde{\mathbf{H}}_t$ is the $N_R[t] \times N_f$ measurement matrix resulting from the ordered concatenation of the N_f column vectors $\{\tilde{\mathbf{H}}_t[n], n = 0, 1, \ldots, N_f - 1\}$,

$$\hat{\mathbf{H}}_t\left(\tilde{h}, \tilde{\theta}, \tilde{\tau}\right) \triangleq \tilde{h} \mathbf{M}_t\left(\tilde{\theta}, \tilde{\tau}\right), \quad (35)$$

$\mathbf{M}_t(\tilde{\theta}, \tilde{\tau})$ represents an $N_R[t] \times N_f$ matrix, whose element lying on its r-th row and its n-th column is defined as

$$m_{t,r,n}(\tilde{\theta}, \tilde{\tau}) \triangleq a_{t,r}\left(\tilde{\theta}, f_n\right) b\left(\tilde{\tau}, f_n\right), \quad (36)$$

and $\{\beta_k^{(l)}, k = 0, 1, \ldots, l\}$ are real parameters (also known as *mixing coefficients*) such that: a) $\beta_k \geqslant 0$ for any k ; b)

$$\sum_{k=0}^{l} \beta_k^{(l)} = 1. \tag{37}$$

M step - In this step, the *three-dimensional* (3D) optimization problem

$$\min_{\tilde{h}, \tilde{\theta}, \tilde{\tau}} \left\| \mathbf{X}_t^{(p)}[k] - \tilde{h}\mathbf{M}_t\left(\tilde{\theta}, \tilde{\tau}\right) \right\|^2 \rightarrow \tilde{h}_k^{(p)}, \tilde{\theta}_k^{(p)}, \tilde{\tau}_k^{(p)} \tag{38}$$

is solved, so generating the new (and, hopefully, more accurate) estimate $(\tilde{\theta}_k^{(p)}, \tilde{\tau}_k^{(p)}, \tilde{h}_k^{(p)})$ of the triplet (θ_k, τ_k, h_k) (with $k = 0, 1, \ldots, l$). This problem can be efficiently solved by first evaluating the minimum of the cost function appearing in eq. (38) with respect to $\tilde{h}$, given the couple $(\tilde{\theta}, \tilde{\tau})$; this produces the estimate

$$\check{h}_k^{(p)}\left(\tilde{\theta}, \tilde{\tau}\right) = \left(n_R[t]N_f\right)^{-1} \cdot \sum_{r=0}^{N_R[t]-1} \sum_{n=0}^{N_f-1} X_{t,r,n}^{(p)}[k] \, m_{t,r,n}^*\left(\tilde{\theta}, \tilde{\tau}\right) \tag{39}$$

of h_k, where $X_{t,r,n}^{(p)}[k]$ denotes the element lying on the r-th row and the n-th column of $\mathbf{X}_t^{(p)}[k]$ (34). Then, setting $\tilde{h} = \check{h}_k^{(p)}(\tilde{\theta}, \tilde{\tau})$ in the RHS of eq. (38) results in the 2D optimization problem

$$\min_{\tilde{\theta}, \tilde{\tau}} \left\| \mathbf{X}_t^{(p)}[k] - \check{h}_l^{(p)}\left(\tilde{\theta}, \tilde{\tau}\right)\mathbf{M}_t\left(\tilde{\theta}, \tilde{\tau}\right) \right\|^2 \rightarrow \tilde{\theta}_q^{(p)}, \tilde{\tau}_q^{(p)}, \tag{40}$$

that can be solved through an exhaustive search over the domain $S_{\tilde{\theta}} \times S_{\tilde{\tau}}$, where $S_{\tilde{\theta}} = [\theta_0, \theta_{N_\theta-1}]$ and $S_\tau \triangleq [2R_m/c, 2R_M/c]$. Once $\tilde{\theta}_q^{(p)}$ and $\tilde{\tau}_q^{(p)}$ become available, $\tilde{h}_q^{(p)} = \check{h}_k^{(p)}(\tilde{\theta}_q^{(p)}, \tilde{\tau}_q^{(p)})$ is computed on the basis of eq. (39). This concludes the M step and, consequently, the p-th iteration of the EMBE. At the end of the last (i.e., of the N_{EM}-th) iteration of the EMBE, the new estimate

$$(\hat{\theta}_k, \hat{\tau}_k, \hat{h}_k) = \left(\tilde{\theta}_k^{(l,N_{EM}+1)}, \tilde{\tau}_k^{(l,N_{EM}+1)}, \tilde{h}_k^{(l,N_{EM}+1)}\right) \tag{41}$$

of the triplet (θ_k, τ_k, h_k) becomes available (with $k = 0, 1, \ldots, l$). Note also that the initialization of the first iteration is simply accomplished by setting $(\tilde{\theta}_k^{(0)}, \tilde{\tau}_k^{(0)}, \tilde{h}_k^{(0)}) = (\hat{\theta}_k, \hat{\tau}_k, \hat{h}_k)$ for $k = 0, 1, \ldots, l$.

The EMBE deserves the following comments:

1. It does not have to be executed at the end of each iteration of the CLEAN algorithm or of the MWLA; for instance, it can employed once the most important targets (i.e., the targets most contributing to the initial energy $E_{\tilde{H}}^{(0)}$; see eqs. (12) and (30)) have been identified. Postponing the parameter refinement based on the EMBE can have a significant impact on the computational cost of the overall estimation procedure.

2. Its *accuracy* and *convergence* are influenced by the values of the mixing coefficients $\{\beta_k^{(l)}, k = 0, 1, \ldots, l\}$. The simplest choice for these coefficients consists in assigning the same value to all of them, so that $\beta_k^{(l)} = 1/(l+1)$ (with $k = 0, 1, \ldots, l$). However, our computer simulations have

evidenced that the estimation accuracy can be improved by selecting

$$\beta_k^{(l)} \propto |\hat{h}_k|^2 \tag{42}$$

for $k = 0, 1, \ldots, l$; in this case, the second term appearing in the RHS of eq. (34) plays a more important role in the case of stronger echoes. Note also that no rule is available for a priori selecting a proper value for the parameter N_{EM}; however, it should be expected that the EMBE convergence becomes slower as l (i.e., as the number of identified targets) increases.

3. Its most computationally intensive task is represented by the solution of the 2D optimization problem (40). The computational complexity of this problem can be mitigated by restricting the search domain from $S_{\tilde{\theta}} \times S_{\tilde{\tau}}$ to $[\tilde{\theta}_q^{(p-1)} - \Delta\theta_{EM}/2, \tilde{\theta}_q^{(p-1)} + \Delta\theta_{EM}/2] \times [\tilde{\tau}_q^{(p-1)} - \Delta\tau_{EM}/2, \tilde{\tau}_q^{(p-1)} + \Delta\tau_{EM}/2]$, where the parameter $\Delta\theta_{EM}$ ($\Delta\tau_{EM}$) represents the size of the new azimuth (delay) domain (the correspondig size for the range domain is $\Delta R_{EM} = 2c/\Delta\tau_{EM}$); the resolutions adopted for the range and the azimuth over the new domain are denoted R_{res} and θ_{res}, respectively. This strategy is motivated by the fact that the quality of the initial estimates provided by the CLEAN algorithm (or by the MWLA) to the EMBE is not usually poor; consequently, it is expected that the new estimates $\tilde{\theta}_q^{(p)}$ and $\tilde{\tau}_q^{(p)}$ generated by the EMBE in its p-th iteration will not be too far from $\tilde{\theta}_q^{(p-1)}$ and $\tilde{\tau}_q^{(p-1)}$, respectively. A potential alternative to this approach is represented by the use of *interpolation techniques* in the search of the local minima of the cost function appearing in eq. (40) (see [34, Sec. IV]); however, this possibility is not discussed further and is left for future research.

E. COMPUTATIONAL COMPLEXITY OF THE PROPOSED ITERATIVE ALGORITHMS

The complexity of all the iterative algorithms described in the previous paragraphs has been carefully assessed in terms of number of *floating operations* (flops) to be executed in the detection of L targets. The general criteria adopted in estimating the computational cost of an algorithm are the same as those illustrated in [35, Appendix A, p. 5420] and are summarised in the Appendix, where a detailed analysis of the costs of the different tasks accomplished by each iterative algorithm is also provided. Our analysis leads to the conclusion that the computational cost of the CLEAN algorithm, of the MWLA, of the EMBE, of the CLEAN combined with the EMBE, of the MWLA combined with the EMBE, and of the MUSIC are approximately of order $\mathcal{O}(N_{CL})$, $\mathcal{O}(N_{MW})$, $\mathcal{O}(N_{EMBE})$, $\mathcal{O}(N_{CLE})$, $\mathcal{O}(N_{MWE})$ and $\mathcal{O}(N_{MU})$, respectively, with

$$N_{CL} = 6N_f N_{\tilde{\theta}} N_{\tilde{\tau}} N_v + 2N_{\tilde{\tau}} N_{\tilde{\theta}} N_f$$
$$+ 2N_{\tilde{\tau}} N_{\tilde{\theta}} N_v + 15N_f N_v \tag{43}$$

$$N_{MW} = N_v^2 \left(6N_f + 8N_\theta\right) + 30N_f N_v$$
$$+ 8N_{\tilde{\tau}} N_f + 30N_{\tilde{\theta}} N_v \tag{44}$$

TABLE 1. Azimuth and range of the targets characterizing scenario # 1, and their estimates computed by three different algorithms (MUSIC, CLEAN and MWLA).

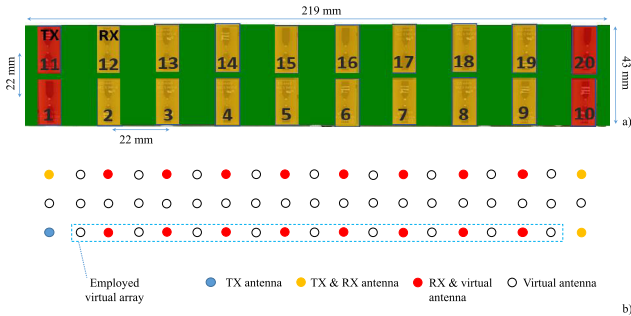| Target	Params	1	2	3	4	5
Exact	$\theta(°)$	-18.0	3.0	13.0	24.0	38.0
	R (cm)	82.5	81.0	82.5	73.5	53.0
MU	$\theta(°)$	-24.0	-2.0	18.0	30.0	43.0
	R (cm)	86.0	85.0	87.5	80.0	58.0
CL	$\theta(°)$	-16.0	2.0	12.0	23.0	35.0
	R (cm)	87.5	85.5	86.5	78.0	54.5
MW	$\theta(°)$	-18.0	3.0	13.0	26.0	41.0
	R (cm)	87.0	84.5	86.5	76.0	53.0

FIGURE 2. a) Physical URA of the employed radar device; b) representation of the associated virtual array and of the portion (enclosed in the dashed rectangle) exploited by our estimation algorithms.

$$N_{EMBE} = L\left[28 N_v N_f N_{\tilde{\tau},EM} N_{\tilde{\theta},EM}\right] + 2L^2 N_v N_f \quad (45)$$

$$N_{CLE} = 6L N_v N_f N_{\tilde{\tau}} N_{\tilde{\theta}} + 28 L N_{EM} N_v N_f N_{\tilde{\tau},EM} N_{\tilde{\theta},EM} \quad (46)$$

$$N_{MWE} = L N_v^2 \left(6 N_f + 8 N_\theta\right) + 28 L N_{EM} N_v N_f N_{\tilde{\tau},EM} N_{\tilde{\theta},EM} \quad (47)$$

and

$$N_{MU} = 17\left(l_1 l_2\right)^3 + 16\left(l_1 l_2\right)^2 \left(p_1 p_2 + N_{\tilde{\tau}} N_{\tilde{\theta}}\right). \quad (48)$$

The parameters l_1, l_2, p_1 and p_2 appearing the last formula are same as those defined in [22, Sec. IV].

IV. NUMERICAL RESULTS

The accuracy of the algorithms illustrated in the previous Section has been assessed in an indoor area of small size, because of the limited power radiated by the radar device employed in our experiments. The numerical results shown in this section refer to two different scenarios. The first scenario is characterized by five targets and, more specifically, by $L = 5$ identical metal discs, all having a diameter equal to 5.5 cm and placed on an horizontal plastic desk. The exact range and azimuth of each of these targets are listed in Table 1. In the second scenario, instead, $L = 4$ equal coins, having a diameter of 2.0 cm, are placed at a uniform distance from our radar device (see Fig. 3); their range and azimuth are listed in Table 3.

The employed radar has been designed and manufactured by *Vayyar Imaging Ltd Company* [36]. It operates in TDM mode and it is equipped with the *uniform rectangular array* (URA) illustrated in Fig. 2-a). This array consists of 20 antennas; moreover, four of them (more precisely, those identified by the numbers 1, 10, 11 and 20) can be employed as TX antennas, whereas those identified by the numbers $2 − 20$ as RX antennas only. The *virtual* array associated with this physical URA is shown in Fig. 2-b) and consists of 53 antennas; however, only the portion enclosed within the dashed rectangle and containing 17 virtual elements (forming a ULA) has been exploited by our estimation algorithms. Moreover, the following values have been selected for the parameters characterizing channel sounding in the frequency domain (see eq. (2)): $f_0 = 5.05$ GHz, $\Delta f = 9.4$ MHz and $N_f = 510$ (so that the overall sweep bandwidth is about 5.0 GHz).

The raw data acquired by our radar over a single snapshot have been processed by the algorithms illustrated in the previous Section. The estimation accuracy of each algorithm has been assessed by evaluating the *root mean square error* (RMSE)

$$\bar{\varepsilon}_X \triangleq \sqrt{L^{-1} \sum_{l=1}^{L} \left[X_l - \hat{X}_l\right]^2} \quad (49)$$

and the peak error

$$\hat{\varepsilon}_X \triangleq \max_l \left|X_l - \hat{X}_l\right| \quad (50)$$

for the range ($X = R$) and the azimuth ($X = \theta$); here, X_l and $\hat{X}_l$ represent the exact value of the parameter to be estimated for the l-th target (with $l = 0, 1, 2, 3$ and 4) and the corresponding estimate. Our assessment of *computational requirements* is based, instead, on assessing both the *computation time* (CT) and the overall computational complexity required for processing the whole set of acquired data and generating the estimates of range and azimuth for all the targets.

The accuracy achieved by the standard beamformer, the CLEAN algorithm and the MWLA in all the considered scenarios has been assessed under the assumption that the number of targets is known a priori; moreover, the following values have been selected for the parameters defining the search domain of these algorithms: a) $\theta_0 = −90°$, $\Delta\theta = 1°$ and $N_\theta = 181$ ($R_m = 20$ cm, $\Delta R = 0.5$ cm, $R_M = 120$ cm and $N_\tau = 201$) for the sequence $\{\theta_k\}$ ($\{R_k\}$) of trial values of the azimuth (range). A contour plot of the cost function $J_t(\tilde{\theta}, \tilde{\tau})$ (9) evaluated by the standard beamformer and the CLEAN algorithm in the first considered scenario is illustrated in Fig. 4; the estimates of the azimuth and of the range computed by the CLEAN algorithm, the MWLA and the 2D MUSIC are listed in Table 1 (the acronyms CL, MW and MU refer to the CLEAN algorithm, the MWLA and the 2D MUSIC algorithm, respectively), together with the exact values of these quantities. The corresponding values of $\bar{\varepsilon}_\theta$ and

FIGURE 3. Measurement setup employed in the second scenario. Four metal coins are placed over a rectangular carton box.
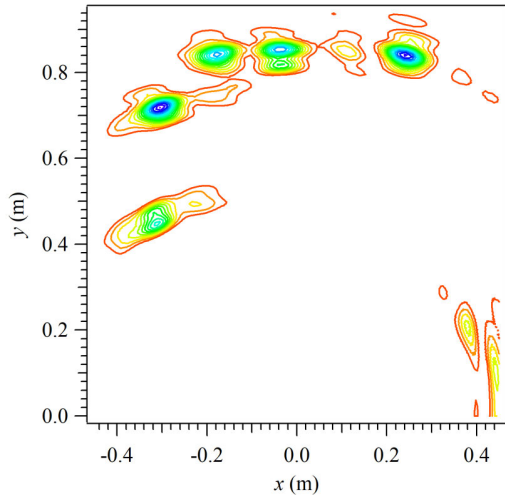

FIGURE 4. Contour plot (in Cartesian coordinates) of the cost function $J_t(\tilde{\theta}, \tilde{\tau})$ (9) evaluated by the standard beamformer for the considered propagation scenario. The peaks associated with the five targets are clearly visible.

FIGURE 5. Computational complexity (black) and computational time (blue) versus the number of targets (*L*).

TABLE 2. Root mean square errors, peak errors and computation times for all the analysed estimation algorithms. Scenario # 1 is considered.

	CL	MW	CLE	MWE	MU
$\bar{\varepsilon}_\theta$ (°)	1.8	1.6	1.8	0.6	5.4
$\bar{\varepsilon}_R$ (cm)	4.1	3.3	4.1	3.5	4.9
$\hat{\varepsilon}_\theta$ (°)	3.0	3.0	3.6	1.7	6.0
$\hat{\varepsilon}_R$ (cm)	5.0	4.5	5.0	4.9	6.5
CT	0.7 s	0.02 s	5.3 s	4.6 s	> 5 h
$GFlops$	9.46	0.01	11.4	2.0	651.7

$\bar{\varepsilon}_R$ ($\hat{\varepsilon}_\theta$ and $\hat{\varepsilon}_R$) computed on the basis of eq. (49) (eq. (50)) are listed in Table 2 for all the considered algorithms and the 2D MUSIC algorithm. These results show that all the estimation algorithms achieve similar accuracies, but the best one is provided by the MWLA, which, luckily, requires the shortest CT. Note also that all the iterative algorithms require a substantially shorter CT than the MUSIC algorithm. It is also worth mentioning that the MWLA offers a substantial advantage in terms of computational complexity/time even for a different number of targets. This can be easily inferred from Fig. 5, that shows the computational complexity (assessed on the basis of eqs. (43)-(48)) and the CT characterizing all the considered iterative algorithms for a number of targets ranging from 2 to 8 (no result is shown for the MUSIC algorithm since its complexity and computation time are much higher than those
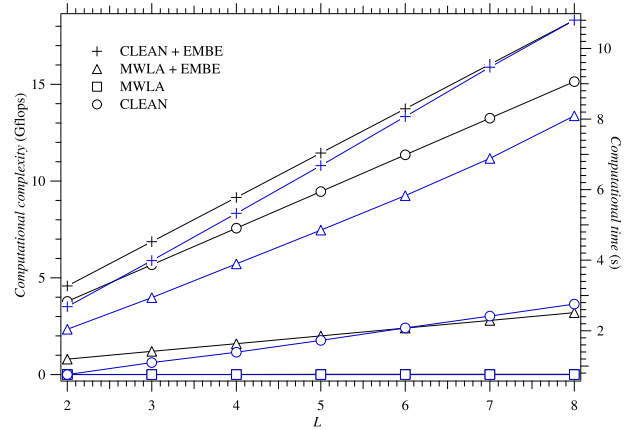
of the other algorithms). The results shown in this figure lead to the following conclusions:

1) The MWLA requires the lowest complexity. This is due to the fact that this algoritm computes the steering vector at the central frequency only and its estimation of targets parameters does not involve the cost function (9).

2) The complexity assessed for the CLEAN algorithm is higher than that of the MWLA combined with the EMBE (MWLA+EMBE), since the most demanding task in the last algorithm involves a limited search domain, as explained at the end of subsection III-D. However, the CT observed for the CLEAN algorithm is lower than that of the MWLA combined with the EMBE (MWLA+EMBE). This is due to the fact the MATLAB implementation of the former algorithm is more efficient than that of the latter one. Note, in particular, that in the latter algorithm the parameters of search domain $S_{\tilde{\theta}} \times S_{\tilde{\tau}}$ (and, consequently, the values of the steering vector) need to be re-computed any time that a new target is found.

The potential improvement in estimation accuracy provided by the EMBE has been also assessed when it is employed at the end of the last (i.e., of the fourth) iteration of the CLEAN algorithm or of the MWLA, and its mixing coefficients are computed on the basis of eq. (42). Moreover, the following values have been selected for the parameters of the EMBE: a) $\Delta R_{EM}/2 = 0.5$ cm and $\Delta\theta_{EM}/2 = 1°$ for the size of the search domain (the adopted resolutions are $R_{res} = 0.1$ cm and $\theta_{res} = 0.1°$ for the range and the azimuth variables, respectively); b) $N_{EM} = 5$ for the overall number of iterations. The estimation accuracies $\bar{\varepsilon}_\theta$ and $\bar{\varepsilon}_R$ achieved by combining the EMBE with the CLEAN algorithm and with

TABLE 3. Azimuth and range of the targets characterising scenario # 2, and their estimates computed by five different algorithms (MUSIC, CLEAN, MWLA, CLEAN + EMBE and MWLA + EMBE).

Target	Params	1	2	3	4	$\bar{\varepsilon}$	$\hat{\varepsilon}$	CT (s)
Exact	$\theta(°)$	-15.0	-3.0	8.0	25.0			
	R (cm)	65.0	65.0	65.0	65.0			
MU	$\theta(°)$	-14.0	-2.0	6.0	23.0	1.5	2.0	> 5 h
	R (cm)	66.0	67.0	68.0	70.0	3.0	5.0	> 5 h
CL	$\theta(°)$	-15.0	-2.0	7.0	22.0	1.6	3.0	0.5
	R (cm)	66.0	67.0	67.0	70.0	3.0	5.0	0.5
MW	$\theta(°)$	-16.0	-3.0	7.0	25.0	0.7	1.0	0.01
	R (cm)	67.0	67.0	67.0	68.0	2.0	3.0	0.01
CLE	$\theta(°)$	-15.3	-1.9	7.5	21.8	2.2	3.0	3.9
	R (cm)	66.0	67.0	67.0	70.0	3.0	5.0	3.9
MWE	$\theta(°)$	-15.8	-2.7	7.2	23.4	0.9	1.0	3.4
	R (cm)	66.0	67.0	68.0	69.0	3.0	3.0	3.4

TABLE 4. Azimuth and range of the targets in the considered six configurations (all related to scenario # 2).

Target	Params	1	2	3	4
Exp. 1	$\theta(°)$	-11.0	4.0		
	R (cm)	65.0	65.0		
Exp.2	$\theta(°)$	-25.0	-13.0	4.0	
	R (cm)	65.0	65.0	65.0	
Exp. 3	$\theta(°)$	-25.0	-13.0	4.0	19.0
	R (cm)	65.0	65.0	65.0	65.0
Exp. 4	$\theta(°)$	-3.0	8.0		
	R (cm)	65.0	65.0		
Exp. 5	$\theta(°)$	-3.0	8.0	20.0	
	R (cm)	65.0	65.0	65.0	
Exp. 6	$\theta(°)$	-15.0	-3.0	8.0	25.0
	R (cm)	65.0	65.0	65.0	65.0

TABLE 5. Average of root mean square errors and peak errors for all the investigated estimation algorithms. The six configurations described in Table 4 are considered for target geometry.

	CL	MW	CLE	MWE	MU
$\bar{\varepsilon}_\theta$ (°)	1.4	1.2	1.7	1.2	1.3
$\bar{\varepsilon}_R$ (cm)	2.0	2.0	2.0	2.0	1.8
$\hat{\varepsilon}_\theta$ (°)	2.0	1.5	2.0	1.5	1.5
$\hat{\varepsilon}_R$ (cm)	2.8	2.8	2.8	2.8	3.0

again, the best accuracy/CT tradeoff. Moreover, the use of the EMBE in combination with the CLEAN algorithm or with the MWLA provides some local improvement in the estimation of the position of the targets; however, no significant variation in terms of RMSE and peak errors is observed. Another interesting result found in this scenario is represented by the fact that the MWLA exhibits a good accuracy (better than that of the other algorithms) even if the azimuth of the targets is not small (e.g., the azimuth of the fourth target is equal to 25.0°).

Further numerical results about multiple variants of the second scenario are given in Table 5. In this case, the number of targets, that are all placed at a uniform distance (equal to 65 cm) from the radar device, ranges from two to four and a uniform angular spacing between adjacent targets is selected. Moreover, six distinct configurations for the target geometry are considered (the range and azimuth of each target are given in Table 4). The RMSEs and the peak errors resulting from an average over the considered six configurations are listed in Table 5. From these results it is easily inferred that the iterative algorithms perform well and the best accuracy is achieved again by the MWLA.

The last technical issue analysed in detail in our computer simulation is represented by the behaviour of the residual energy $E_{\hat{H}}^{(l)}$ (30) available at the end of the *l*-th iteration in the CLEAN algorithm and in the MWLA. Some results referring to the first scenario are shown in Fig. 6. Note that, in this case, two distinct sets of values are given for each algorithm, one computed on the basis of the raw data acquired by our radar (i.e., of the *experimental* data), the other one evaluated on the basis of computer generated data (i.e., of *simulated* data); in the last case, five *point targets*, whose azimuth and range are the same as those given in Table 1, have been assumed. From these results it is easily inferred that the iterative cancellation procedure accomplished by the CLEAN algorithm results in a steep descrease of the residual energy in the simulated case. This suggests that a stopping criterion based on the inequality (31) could be really used in this case. However, a substantially smaller rate of decrease is observed for the residual energy of the CLEAN algorithm in the case of experimental data. This is mainly due to the fact that the metal discs employed in our experiments cannot be represented as point targets; for this reason, multiple echoes are received by the radar device from the same target. As a matter of fact, when experimental data are processed by the CLEAN algorithm, new echoes, very close to those already identified, appear if its cancellation procedure proceeds beyond the 4-th iteration. A gap between the
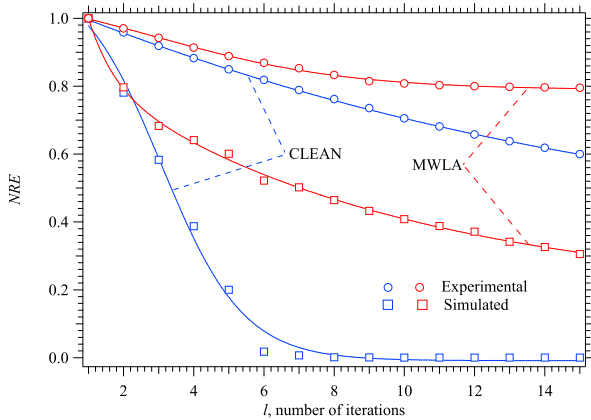
the MWLA are listed in Table 2 (where the acronyms CLE and MWE refer to the combination of the CLEAN algorithm with the EMBE, and to that of the MWLA with the EMBE, respectively). From these results it is easily inferred that:

1) Combining the CLEAN algorithm with the EMBE does not result in a better accuracy in range estimation, and slightly improves the accuracy of azimuth estimates.

2) The best accuracy in azimuth estimation is obtained by combining the MWLA with the EMBE; in fact, this reduces the azimuth RMSE from 1.6° to 0.6°. This improvement can be related to the fact that the MWLA benefits from the *beamforming* expressed by eq. (39) and accomplished by the EMBE in estimating h_k, given the trial values $\tilde{\theta}$ and $\tilde{\tau}$ of the target azimuth and delay, respectively.

Our computer simulations have also evidenced that, if the EMBE is used at the end of each iteration of the CLEAN algorithm (or of the MWLA), no real improvement is obtained and the computation time becomes substantially larger.

Let us focus now on the second scenario. In this case, the estimates of the azimuth and of the range computed by all the analysed algorithms, together with the corresponding RMSEs, peak errors and CTs, are listed in Table 3. These results lead to the conclusion that the MWLA achieves, once

FIGURE 6. Normalized residual energy evaluated for the CLEAN algorithm and the MWLA algorithm for the considered propagation scenario. Both experimental and simulated data are considered.

residual energy computed on the basis of the simulated data and that referring to the experimental data is also observed in the case of the MWLA. However, the rate of decrease is substantially smaller than that evalauted in the case of the CLEAN algorithm in both cases. This depends on the fact that the steering vector $\mathbf{a}_t(\hat{\theta}_{l-1}, f_r)$ is evaluated at the reference frequency f_r only in the computation of the residual $\tilde{\mathbf{H}}_t^{(l)}[n]$ (32) for any n; this unavoidably introduces an error. These results suggest that, if the MWLA is employed, the stopping criterion based on the inequality (31) can be still used, but the threshold $\varepsilon_{\tilde{H}}$ has to be selected very carefully. Despite this problem, we believe that the MWLA and the combination of the MWLA with EMBE represent the best options for range and azimuth estimation in SFCW MIMO radars.

Finally, it is worth mentioning that, in our measurement campaigns, other scenarios, characterized by a different numbers of metal discs and target coordinates, have been also considered. However, accuracies similar to the ones measured for the two scenarios described above have been found, provided that the angular coordinates of the employed targets were contained in a limited domain. In fact, it is well known that the angular resolution $\Delta\theta$ of a MIMO radar decreases proportionally with the deviation of the target direction from the boresight of the employed array; more specifically, it can be shown that (see [37, Eq.(14), Sec. II])

$$\Delta\theta = \frac{\lambda}{2D(N_R \cdot N_T - 1) \cdot cos(\theta)} \quad (51)$$

where D is the spacing of adjacent virtual elements, N_R (N_T) is the number of receive (transmit antennas) and θ is the direction of arrival (azimuth) of the impinging signal.

V. CONCLUSIONS

In this paper, five techniques for jointly estimating ranges and DOA's in a MIMO SFCW radar system have been described. All these techniques are deterministic and estimate target parameters through iterative cancellation procedures. Our numerical results, based on real measurements, evidence that, in a 2D scenario, the range and azimuth estimates computed

by all algorithms are reasonably accurate. However, on the one hand, the MWLA achieves a slightly better accuracy and requires a smaller computational effort than the CLEAN algorithm; on the other hand, limited or no improvement is found if the estimates generated by these techniques are processed by an EM-based algorithm for refining them. Our ongoing work concerns the extension of these techniques to a 3D propagation scenario.

APPENDIX

In this Appendix, the computational complexity, in terms of flops, is assessed for the deterministic techniques illustrated in this paper and for the MUSIC technique. The general criteria adopted in estimating the computational cost of each algorithm are the same as those illustrated in [35, Appendix A, p. 5420] and [38] and can be summarised as follows:

- $2d - 1$ flops are required to compute the inner product $\mathbf{u}^T \mathbf{v}$ of two $d \times 1$ real column vectors;
- $6d + 2(d - 1)$ flops are required to compute the inner product $\mathbf{u}_c^T \mathbf{v}_c$ of two $d \times 1$ complex vectors;
- $m[6n + 2(n - 1)]p$ flops are required to compute the product between two complex matrices $\mathbf{A} \in \mathbb{C}^{m \times n}$ and $\mathbf{B} \in \mathbb{C}^{n \times p}$;
- d flops are required to find the maximum element of a vector $\mathbf{v} \in \mathbb{R}^{1 \times d}$;
- $\mathcal{O}(n^3)$ flops are required in a single iteration of the QR algorithm employed for the computation of the eigenvalues of a square matrix $\mathbf{A} \in \mathbb{C}^{n \times n}$.

A. COMPUTATIONAL COMPLEXITY OF THE CLEAN ALGORITHM

The overall computational cost of each iteration of the CLEAN algorithm can be expressed as

$$\mathcal{C}_{CL} = \mathcal{C}_s + \mathcal{C}_{pd} + \mathcal{C}_{pc} + \mathcal{C}_{ec}, \quad (52)$$

where

$$\mathcal{C}_s = N_{\tilde{\theta}} N_{\tilde{\tau}} \left[2(N_f - 1) + 2(N_v - 1) + 6N_f N_v \right] \quad (53)$$

is the contribution due to the evaluation of the cost function of the standard beamformer (see eq. (9)), $N_v = N_T \cdot N_R$ is the overall number of virtual elements of radar array,

$$\mathcal{C}_{pd} = N_\theta + N_\tau \quad (54)$$

is the contribution of the search of a single maximum $(\hat{\theta}_l, \hat{\tau}_l)$ of the cost function in eq. (9),

$$\mathcal{C}_{pc} = N_f(6N_v + 2N_v) \quad (55)$$

is the contribution of the cancellation produre expressed by eq. (17), and

$$\mathcal{C}_{ec} = N_f (6N_v + N_v - 1) + N_f - 1 \quad (56)$$

is the contribution due to the computation of the residual energy (see eq. (30)). Substituting eqs. (53)-(56) in eq. (52) and keeping only the most relevant terms leads to eq. (43).

B. COMPUTATIONAL COMPLEXITY OF THE MWLA
The overall computational cost of each iteration of the MWLA can be expressed as

$$\mathcal{C}_{MW} = \mathcal{C}_r + \mathcal{C}_{ct} + \mathcal{C}_v + \mathcal{C}_\tau + \mathcal{C}_B \\ + \mathcal{C}_{ft} + \mathcal{C}_h + \mathcal{C}_{pc} + \mathcal{C}_{ec}, \quad (57)$$

where

$$\mathcal{C}_r = 6N_f N_v^2 + 2N_v(N_f - 1) \quad (58)$$

is the contribution due to the computation of the covariance matrix $\mathbf{R}_{xx}^{(l)}$ (18),

$$\mathcal{C}_{ct} = N_{\tilde{\theta}}\left(22N_v + 8N_v^2 - 2\right) \quad (59)$$

is the contribution of the optimization problem expressed by eq. (33) (this includes also the computation of the norm $||\mathbf{a}_t(\tilde{\theta}, f_r)||$),

$$\mathcal{C}_v = 8N_f N_v + 8N_v - 2N_f - 1 \quad (60)$$

is the contribution due to the computation of the matrix $\hat{\mathbf{v}}_{t,k}^{(l)}$ (generated by stacking the N_f row vectors $\{(\hat{\mathbf{u}}_{t,k}^{(l)}[n])^T, n = 0, 1, \ldots, N_f - 1\}$ according to their natural order; see eq. (23)),

$$\mathcal{C}_\tau = 5N_{\tilde{\tau}} + 8N_{\tilde{\tau}}N_f \quad (61)$$

is the contribution due to the computation of the delays $\{\hat{\tau}_k^{(l)}\}$ (see eq. (24)),

$$\mathcal{C}_B = 8N_f N_v + 8N_f - 2N_v - 2 \quad (62)$$

is the contribution due to the computation of the matrix $\hat{\mathbf{B}}_t^{(l)}$ (see eq. (26))

$$\mathcal{C}_{ft} = 5N_{\tilde{\theta}} + 8N_{\tilde{\theta}}N_v \quad (63)$$

is the contribution due to the refinement of the fine estimates $\{\hat{\theta}_k^{(l)}\}$ (see eq. (25)),

$$\mathcal{C}_h = 17N_v - 1 \quad (64)$$

is the contribution due to the computation of the complex gains $\{\hat{h}_k^{(l)}\}$ (see eq. (29)), $\mathcal{C}_{pc}$ is the cost of the cancellation procedure expressed by eq. (32), and $\mathcal{C}_{ec}$ is the contribution due to the computation of the residual energy $E_{\tilde{H}}^{(l)}$ (see eq. (30)).

Substituting eqs. (58)-(64) in eq. (57) and keeping only the most relevant terms leads to eq. (44).

C. COMPUTATIONAL COMPLEXITY OF THE EMBE
The overall computational cost of a single iteration of EMBE in the presence of L targets can be expressed

$$\mathcal{C}_{EM} = \mathcal{C}_x + \mathcal{C}_M + \mathcal{C}_{h,EM} + \mathcal{C}_o, \quad (65)$$

where

$$\mathcal{C}_x = 2(L + 2)N_v N_f \quad (66)$$

is the contribution due to the computation of the $N_R[t] \times N_f$ matrices $\{\mathbf{X}_t^{(p)}[k]\}$ (see eq. (34)),

$$\mathcal{C}_M = 6N_v N_f N_{\tilde{\theta},EM} N_{\tilde{\tau},EM} \quad (67)$$

is the contribution due to the evaluation of the function $\mathbf{M}_t(\tilde{\theta}, \tilde{\tau})$ in eq. (36) ($N_{\tilde{\theta},EM}$ and $N_{\tilde{\tau},EM}$ denote the size of the sets $S_{\tilde{\theta},EM}$ and $S_{\tilde{\tau},EM}$, respectively),

$$\mathcal{C}_{h,EM} = N_{\tilde{\theta},EM}N_{\tilde{\tau},EM}\left[6N_vN_f + 2(N_f - 1)\right] \\ + 2N_{\tilde{\theta},EM}N_{\tilde{\tau},EM}(N_v - 1) + 2 \quad (68)$$

is the contribution due to the evaluation of the complex amplitude $\check{h}_k^{(p)}\left(\tilde{\theta}, \tilde{\tau}\right)$ (39) and

$$\mathcal{C}_o = (16N_vN_f - 2)N_{\tilde{\tau},EM}N_{\tilde{\theta},EM} + N_{\tilde{\theta},EM} + N_{\tilde{\tau},EM} \quad (69)$$

is the contribution originating from the optimization problem (38).

Substituting eqs. (66)-(69) in eq. (65) and keeping only the most relevant terms results in eq. (45).

D. COMPUTATIONAL COMPLEXITY OF COMBINED ALGORITHMS
If the CLEAN algorithm and the MWLA are combined with the EMBE algorithm, the overall computational costs are

$$\mathcal{C}_{CLE} = L\mathcal{C}_{CL} + N_{EM}\mathcal{C}_{EM} \quad (70)$$

and

$$\mathcal{C}_{MWE} = L\mathcal{C}_{MW} + N_{EM}\mathcal{C}_{EM}, \quad (71)$$

respectively (it is assumed that at least L targets are known); here, N_{EM} represents the number of iterations required by the EMBE for the refinement of the estimated parameters. The costs $\mathcal{C}_{CL}$, $\mathcal{C}_{MW}$ and $\mathcal{C}_{EM}$ appearing in the last two formulas are given by eqs. (52), (57) and (65), respectively; substituting the expressions of these costs in eqs. (70) and (71) and keeping only the most relevant terms yields eq. (46) and eq. (47), respectively.

E. COMPUTATIONAL COMPLEXITY OF THE MUSIC ALGORITHM
Our assessment of the computational complexity of the MUSIC algorithm is based on the detailed description given in [22, Sec. IV]; for this reason, the notation employed in that paper is adopted in this paragraph. The overall computational cost of this algorithm can be expressed

$$\mathcal{C}_{MU} = \mathcal{C}_x + \mathcal{C}_e + \mathcal{C}_M, \quad (72)$$

where

$$\mathcal{C}_x = 2(l_1 l_2)^2(8l_1 l_2 + 8p_1 p_2 - 4) \quad (73)$$

is the contribution due to the computation of the data smoothed covariance matrix $\mathbf{C}$ (see [22, Sec. IV, Eq. (12)]),

$$\mathcal{C}_e \approx (l_1 l_2)^3 \quad (74)$$

is the contribution related with the computation of the eigenvalues of the matrix $\mathbf{C}$ and

$$\mathcal{C}_M = 2N_{\tilde{\tau}}N_{\tilde{\theta}}\left[8(l_1l_2)^2 - l_1l_2\left(8L - 2\right) + L - 1\right] \quad (75)$$

is the contribution due to the evaluation of the 2D-MUSIC spectrum (see [22, Sec. IV, Eq. (14)]). Substituting

eqs. (73)-(75) in eq. (72) and keeping only the most relevant terms leads to eq. (48).

Finally, it is important to point out that:

a) In principle, the size of the window (l_1, l_2) and the size (p_1, p_2) of the remaining part of the sampled matrix $\mathbf{X}$, computed on the basis of radar measurements (see [22, Eq. (11), Sec. IV]) and characterized by a size $N_f \times N_v$ in our implementation, can be freely selected. In our work, $l_1 = 14$, $l_2 = 250$, $p_1 = N_v - l_1 + 1$ and $p_2 = N_f - l_2 + 1$ have been chosen.

b) The cost $\mathcal{C}_M$ (72), unlike that of the other algorithms considered in our work, does not depend linearly on L.

ACKNOWLEDGMENT

REFERENCES

[1] E. Fishler, A. Haimovich, R. Blum, L. Cimini, D. Chizhik, and R. Valenzuela, "Performance of MIMO radar systems: Advantages of angular diversity," in *Proc. 38th Asilomar Conf. Signals, Syst., Comput.*, vol. 1. Nov. 2004, pp. 305–309.

[2] J. Li, P. Stoica, and X. Zheng, "Signal synthesis and receiver design for MIMO radar imaging," *IEEE Trans. Signal Process.*, vol. 56, no. 8, pp. 3959–3968, Aug. 2008.

[3] D. W. Bliss and K. W. Forsythe, "Multiple-input multiple-output (MIMO) radar and imaging: Degrees of freedom and resolution," in *Proc. IEEE Conf. Rec. 37th Asilomar Conf. Signals, Syst. Comput.*, vol. 1. Nov. 2003, pp. 54–59.

[4] I. Bekkerman and J. Tabrikian, "Target detection and localization using MIMO radars and sonars," *IEEE Trans. Signal Process.*, vol. 54, no. 10, pp. 3873–3883, Oct. 2006.

[5] F. C. Robey, S. Coutts, D. Weikle, J. C. McHarg, and K. Cuomo, "MIMO radar theory and experimental results," in *Proc. Conf. Rec. 38th Asilomar Conf. Signals, Syst. Comput.*, vol. 1, Nov. 2004, pp. 300–304.

[6] J. Li and P. Stoica, "MIMO radar with colocated antennas," *IEEE Signal Process. Mag.*, vol. 24, no. 5, pp. 106–114, Sep. 2007.

[7] J. Li, L. Xu, P. Stoica, K. W. Forsythe, and D. W. Bliss, "Range compression and waveform optimization for MIMO radar: A Cramér–Rao bound based study," *IEEE Trans. Signal Process.*, vol. 56, no. 1, pp. 218–232, Jan. 2008.

[8] C. Shi, F. Wang, M. Sellathurai, and J. Zhou, "Transmitter subset selection in FM-based passive radar networks for joint target parameter estimation," *IEEE Sensors J.*, vol. 16, no. 15, pp. 6043–6052, Aug. 2016.

[9] C. G. Shi, S. Salous, F. Wang, and J. J. Zhou, "Modified Cramér–Rao lower bounds for joint position and velocity estimation of a Rician target in OFDM-based passive radar networks," *Radio Sci.*, vol. 52, no. 1, pp. 15–33, Jan. 2017.

[10] C. G. Shi, F. Wang, S. Salous, and J. J. Zhou, "Cramér–Rao lower bounds for joint target parameter estimation in FM-based distributed passive radar network with antenna arrays," *Radio Sci.*, vol. 53, no. 3, pp. 314–333, Mar. 2018.

[11] Z. Zhang and Y. Tian, "A novel resource scheduling method of netted radars based on Markov decision process during target tracking in clutter," *EURASIP J. Adv. Signal Process.*, vol. 2016, no. 1, p. 16, Dec. 2016.

[12] H. Rohling and M. M. Meinecke, "Waveform design principles for automotive radar systems," in *Proc. Int. Conf. Radar CIE*, Oct. 2001, pp. 1–4.

[13] M. Richards, *Fundamentals of Radar Signal Processing*. New York, NY, USA: McGraw-Hill, 2014.

[14] F. Gumbmann and A. Schiessl, "Short-range imaging system with a nonuniform SFCW approach," *IEEE Trans. Microw. Theory Techn.*, vol. 65, no. 4, pp. 1345–1354, Apr. 2017.

[15] S. Shirodkar, P. Barua, D. Anuradha, and R. Kuloor, "Heart-beat detection and ranging through a wall using ultra wide band radar," in *Proc. Int. Conf. Commun. Signal Process.*, Calicut, India, Feb. 2011, pp. 579–583.

[16] E. Lagunas, M. G. Amin, and F. Ahmad, "Through-the-wall radar imaging for heterogeneous walls using compressive sensing," in *Proc. 3rd Int. Workshop Compressed Sens. Theory Appl. Radar, Sonar Remote Sens. (CoSeRa)*, Pisa, Italy, Jun. 2015, pp. 94–98.

[17] Azizah, A. B. Suksmono, and A. Munir, "Signal processing of range detection for SFCW radars using Matlab. and GNU radio," in *Proc. Int. Conf. Comput., Control, Inform. Appl. (IC3INA)*, Oct. 2014, pp. 145–148.

[18] B. Kim, S. Kim, and J. Lee, "A novel DFT-based doa estimation by a virtual array extension using simple multiplications for FMCW radar," *Sensors*, vol. 18, no. 5, p. 1560, May 2018.

[19] H. Lv, T. Jiao, Y. Zhang, F. Liang, F. Qi, and J. Wang, "A novel method for breath detection via stepped-frequency continuous wave ultra-Wideband (SFCW UWB) radars based on operational bandwidth segmentation," *Sensors*, vol. 18, no. 11, p. 3873, Nov. 2018.

[20] X. Chen, B. Chen, J. Guan, Y. Huang, and Y. He, "Space-range-Doppler focus-based low-observable moving target detection using frequency diverse array MIMO radar," *IEEE Access*, vol. 6, pp. 43892–43904, 2018.

[21] R. O. Schmidt, "Multiple emitter location and signal parameter estimation," *IEEE Trans. Antennas Propag.*, vol. AP-34, no. 3, pp. 276–280, Mar. 1986.

[22] F. Belfiori, W. van Rossum, and P. Hoogeboom, "Coherent MUSIC technique for range/angle information retrieval: Application to a frequency-modulated continuous wave MIMO radar," *IET Radar, Sonar Navigat.*, vol. 8, no. 2, pp. 75–83, Feb. 2014.

[23] R. Roy and T. Kailath, "ESPRIT-estimation of signal parameters via rotational invariance techniques," *IEEE Trans. Acoust., Speech, Signal Process.*, vol. 37, no. 7, pp. 984–995, Jul. 1989.

[24] J. A. Högbom, "Aperture synthesis with a non-regular distribution of interferometer baselines," *Astron. Astrophys. Suppl.*, vol. 15, p. 417, Jun. 1974.

[25] D. Zankl, S. Schuster, R. Feger, and A. Stelzer, "What a blast!: A massive MIMO radar system for monitoring the surface in steel industry blast furnaces," *IEEE Microw. Mag.*, vol. 18, no. 6, pp. 52–69, Sep./Oct. 2017.

[26] M. Wax and A. Leshem, "Joint estimation of time delays and directions of arrival of multiple reflections of a known signal," *IEEE Trans. Signal Process.*, vol. 45, no. 10, pp. 2477–2484, Oct. 1997.

[27] I. Ziskind and M. Wax, "Maximum likelihood localization of multiple sources by alternating projection," *IEEE Trans. Acoust., Speech Signal Process.*, vol. 36, no. 10, pp. 1553–1560, Oct. 1988.

[28] T. K. Moon, "The expectation-maximization algorithm," *IEEE Signal Process. Mag.*, vol. 13, no. 6, pp. 47–60, Nov. 1996.

[29] M. A. Richards, *Fundamentals of Radar Signal Processing*. New York, NY, USA: McGraw-Hill, 2005.

[30] F. Engels, P. Heidenreich, A. M. Zoubir, F. K. Jondral, and M. Wintermantel, "Advances in automotive radar: A framework on computationally efficient high-resolution frequency estimation," *IEEE Signal Process. Mag.*, vol. 34, no. 2, pp. 36–46, Mar. 2017.

[31] M. Wax and I. Ziskind, "Detection of the number of coherent signals by the MDL principle," *IEEE Trans. Acoust., Speech Signal Process.*, vol. 37, no. 8, pp. 1190–1196, Aug. 1989.

[32] H. Akaike, "Information theory and an extension of the maximum likelihood principle," in *Proc. 2nd Int. Symp. Inf. Theory*, 1973, pp. 267–281.

[33] M. Feder and E. Weinstein, "Parameter estimation of superimposed signals using the EM algorithm," *IEEE Trans. Acoust., Speech Signal Process.*, vol. 36, no. 4, pp. 477–489, Apr. 1988.

[34] J. Selva, "Efficient wideband DOA estimation through function evaluation techniques," *IEEE Trans. Signal Process.*, vol. 66, no. 12, pp. 3112–3123, Jun. 2018.

[35] B. Ait-El-Fquih and I. Hoteit, "A variational Bayesian multiple particle filtering scheme for large-dimensional systems," *IEEE Trans. Signal Process.*, vol. 64, no. 20, pp. 5409–5422, Oct. 2016.

[36] Vayyar Imaging Ltd. *Vayyar*. [Online]. Available: https://vayyar.com/

[37] Y. Huang and P. V. Brennan, "FMCW based MIMO imaging radar for maritime navigation," *Prog. Electromagn. Res.*, vol. 115, pp. 327–342, Apr. 2011.

[38] G. H. Golub and C. F. Van Loan, *Matrix Computations*, 3rd ed. Baltimore, MD, USA: Johns Hopkins University Press, 1996.

EMILIO SIRIGNANO received the B.Sc. and M.Sc. degrees in electrical engineering from the University of Naples "Federico II", Italy, in 2009 and 2013, respectively, and the Ph.D. degree in information and communications technologies (ICT) from the University of Modena and Reggio Emilia, Italy, in 2018. From October 2013 to June 2014, he was a Graduate Researcher with the Electronics Research Group, Delft University, The Netherlands. He is currently a Research Assistant with the Department of Engineering "Enzo Ferrari", University of Modena and Reggio Emilia. His research interests include statistical signal processing and sensor array processing.

GIORGIO M. VITETTA received the Dr.-Ing. degree *(cum laude)* in electronic engineering and the Ph.D. degree from the University of Pisa, Italy, in 1990 and 1994, respectively. Since 2001, he has been a Full Professor of telecommunications with the University of Modena and Reggio Emilia. He has coauthored more than 100 articles published on international journals and on the proceedings of international conferences, and the book on *Wireless Communications: Algorithmic Techniques* (John Wiley, 2013). His current research interests include wireless and wired data communications, localization systems, MIMO radars, and the smart grid. He has served as an Area Editor for the IEEE Transactions on Communications, and also as an Associate Editor for the IEEE Wireless Communications Letters and the IEEE Transactions on Wireless Communications.

ALESSANDRO DAVOLI received the B.S. and M.S. degrees *(cum laude)* in electronic engineering from the University of Modena and Reggio Emilia, Italy, in 2016 and 2018, respectively. He is currently pursuing the Ph.D. degree in automotive for an intelligent mobility with The University of Bologna. His research interests include MIMO radars, with emphasis on the development of novel detection and estimation algorithms for automotive applications.

FEDERICO VIAPPIANI was born in Castelnovo ne' Monti, Italy, in 1994. He received the B.S. and M.S. degrees *(cum laude)* in electronic engineering from the University of Modena and Reggio Emilia, Italy, in 2016 and 2018, respectively.

• • •